

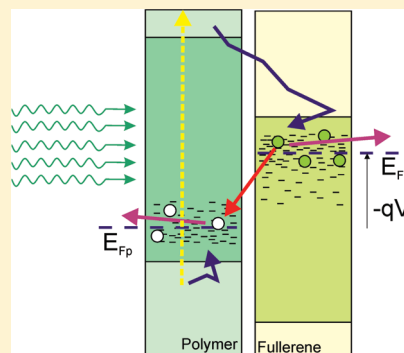
On Voltage, Photovoltage, and Photocurrent in Bulk Heterojunction Organic Solar Cells

Juan Bisquert* and Germà Garcia-Belmonte

Grup de Dispositius Fotovoltaics i Optoelectrònics, Departament de Física, Universitat Jaume I, 12071 Castelló, Spain

Supporting Information

ABSTRACT: The interpretation of voltage, photovoltage, and photocurrent in polymer/fullerene bulk heterojunction (BHJ) solar cells is discussed in terms of fundamental device models and results of capacitance spectroscopy. First we establish the relationship between the applied voltage (which is the difference of Fermi levels) and the variation of electrostatic potential that governs the drift field. We then show the most common distribution of carriers and Fermi levels in the blend layer, supported on experimental results of impedance spectroscopy of P3HT:PCBM solar cells. We arrive at the conclusion that charge separation and charge transportation has very little to do with a built-in electric field between metal contacts, while kinetics plays a major role in photocurrent production. Finally, we discuss the key factors relevant to understand device properties and power conversion efficiencies of the BHJ solar cells: recombination, charge generation, and the current–potential curve, based on the suggested model that emphasizes mobile electrons and holes (that we term quasifree carriers) contributing to the respective Fermi levels.



Solar cells based on a combination of two energetically offset organic materials that donate and accept photogenerated electrons have been investigated for more than two decades¹ and presently constitute a viable device for the production of electricity from sunlight. A widely investigated configuration of the organic solar cell is the bulk heterojunction (BHJ) device, which consists of a blend of an electron acceptor, usually a fullerene that is functionalized to improve the morphology and processing, and a light absorbing polymer that is also a good hole transporter. The two phases in the blend form small aggregates of the order of several nanometers, to facilitate rapid charge separation of electron and holes. Furthermore, each phase should be continuously connected for the transport of the respective charge carrier to separate electrodes. A widely studied BHJ device is the mixture poly(3-hexylthiophene):1-(3-methoxycarbonyl)propyl-1-phenyl[6,6]C₆₁ (P3HT:PCBM), that when optimized, reaches a power conversion efficiency (PCE) of about 5% at 1 sun (AM1.5G irradiation with total power of 100 mW cm⁻²).^{2,3} Recently, a new class of polymers with both lower bandgap and lower energy levels,^{4,5} in combination with fullerenes that assist light absorption and carrier generation,⁶ have provided improved PCE of 8%.

It has been established that the morphology of the blend needs to be controlled and optimized to obtain high rates of carrier creation and separation, and to enhance the long-term stability of the device. However, different polymers impose different requirements for the conformation of the blend. Thermal annealing of P3HT:PCBM blend enhances the efficiency,⁷ by the formation of both highly crystalline regions and a good connectivity.² In contrast to these, in the PTB:PCBM [PTB = poly(thienothiophene-benzodithiophene)] solar cells, the thermal annealing treatment

notably decreases the PCE.⁸ In these PTB low bandgap polymers, formed with alternating ester-substituted thieno(3,4-b)-thiophene and dialkoxyl benzodithiophene units, a high miscibility occurs between the polymer donor and PCBM acceptor up to the molecular level, and larger phase aggregation only reduces the current generation.⁸ Similar effects occur in other polymers as well.⁹

Another important question is the role and optimization of the contacts to the blend. Since the polymer:PCBM blend is macroscopically homogeneous, the contacts have to be selective to extract only one kind of carrier at each side of the active organic layer.¹⁰ Therefore it is necessary to use a combination of a low work function material in one side, that will extract electrons, and a higher work function material that will make a good contact to holes. Furthermore, one of the contacts must obviously be optically transparent to the wavelengths that are absorbed by the organic blend.

The dominant choice for the hole-extracting contact is indium-doped tin oxide (ITO), covered with a thin (5–20 nm) hole-selective layer of PEDOT:PSS, which is a conjugated polymer formed by a mixture of two ionomers, poly(3,4-ethylenedioxythiophene) and poly(styrenesulfonate)). NiO, a *p*-type conducting oxide, also forms an efficient hole extracting layer on ITO.¹¹ A low work function material such as Ba or Ca is evaporated on the blend layer for electron extraction contact, but these metals are easily oxidized and require robust encapsulation. A proposed solution is the use of thin LiF buffer layers between the active layer and

Received: April 11, 2011

Accepted: July 8, 2011

evaporated Al contacts. Alternatively, *n*-type metal oxide layers (ZnO, TiO₂) are deposited on ITO as electron collecting contacts^{12,13} allowing for less unstable metals such as Ag or Au to be used as back hole collecting electrode. In inverted configurations, MoO₃ is also used as a highly electron-blocking layer, which prevents electrons from flowing across the anode but favors hole injection from P3HT.¹⁴ It is suggested that the inversion of electron and hole selective contacts with respect to spin-coating a P3HT:PCBM active layer produces differences in operation due to vertical phase segregation.^{13,15}

This very brief summary already indicates that characterization and improvement of BHJ devices, as well as the development of test methods for fabrication, opens a large number of issues, concerning the operation of the device, including carrier energetics of the materials and their combinations, morphologies, charge generation, recombination, and transport, toward a good understanding of the factors controlling the photovoltage, the photocurrent, the fill factor, and the stability of the devices. Concepts, models, and measuring methods are essential for this. These subjects have been widely explored in a literature that continues to grow, but many questions are not settled. In this Perspective, we aim to provide a critical discussion of the methods of analysis of polymer/fullerene BHJ solar cells that will hopefully clarify some of the main issues.

In the past decade, models to describe BHJ operation have largely used an assumption whereby the applied voltage directly changes the electrical field across the device. Such a field has the function of either separating excitons into electron and hole carriers, transporting the carriers by drift, or both. The fundamental assumptions leading to such a model are discussed, and a very different alternative is suggested in which the function of the applied voltage is to raise the Fermi level of principally one of the carriers. A detailed view of the BHJ internal operation concerning carrier distribution, contacts, and Fermi level distribution is presented based on the measurement of the chemical capacitance in a standard P3HT:PCBM device. Our results point to the prevalence of the second model, and we suggest therefore that the significance of the electrical field is, in many cases, quite marginal. We finally discuss the implications of this approach, which point to a better understanding of the recombination mechanism, which is the key issue in cells with good charge separation properties.

Fundamentals of a Standard BHJ Model. In the Figure 1 we show a popular model to explain the operation of a BHJ solar cell. Let us first summarize the main content of this model, before we discuss the details that justify this picture. The bands are tilted due to different work functions of the metal contacts. The voltage applied between the contacts modifies the tilt of the band and, consequently, the electrical field across the organic layer, which drives electron and hole carriers in opposite directions. This has some important consequences for models of current generation and photovoltage in BHJ solar cells (see, for example, refs 16–18).

We now see how Figure 1 emerges as well as the main implications of this model. Figure 1a shows the separate components of the device. First, an organic layer is shown with electron energy level E_c (conduction band) and hole energy level E_v (valence band), which can be associated with the acceptor (lowest unoccupied molecular orbital (LUMO) and donor highest occupied molecular orbital (HOMO), respectively). The broadening of electron and hole energy states is considered at a later stage of the discussion. The blend layer is contacted by two metals: one of low work function ϕ_c and another one of large work function ϕ_a .

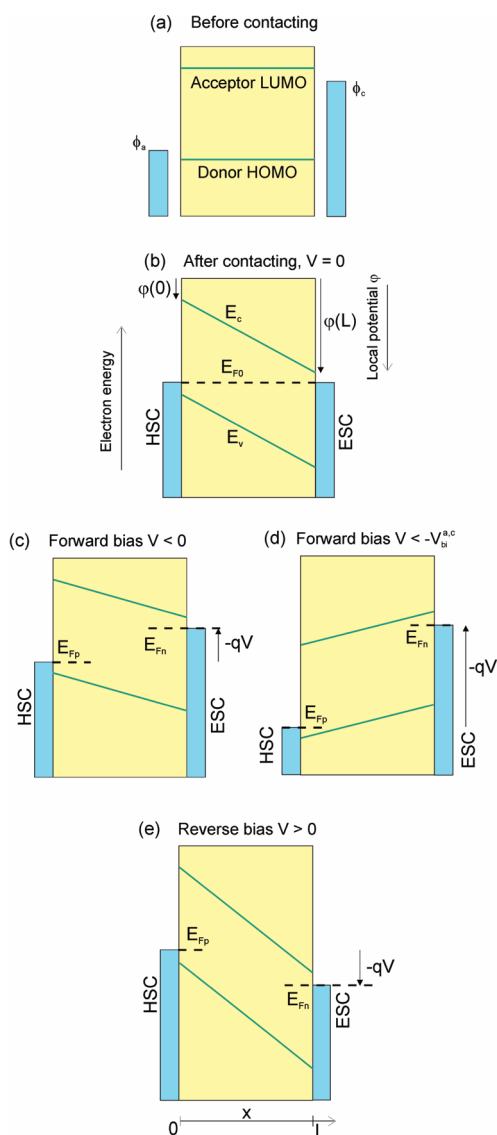


Figure 1. Schematic representation energy diagram of an organic layer with an acceptor LUMO level for electrons E_c and a donor HOMO level for holes E_v , and two contacts: an ESC with work function ϕ_c and an HSC with work function ϕ_a . The contacts are considered as metals in which the carrier energy level is at the Fermi level. All graphs use the assumption of locked density boundary condition (LDBC), in which the density of the carrier extracted is constant at the contact with the metal. (a) The energies of the separate materials and (b–e) different situations of bias voltage V (q is elementary charge) indicating the Fermi levels of electrons (E_{F_n}) and holes (E_{F_p}) close to the respective contacts. In panel b the electrical potential ϕ at the edges of the organic layer is shown.

When the system comes to equilibrium, the Fermi level must be homogeneous, and the situation of Figure 1b is obtained.

Here, and in the rest of this Perspective, the central property of the metal contacts is that the Fermi level accompanies the energy level. Therefore, equalizing the Fermi levels of the metals requires the construction of a difference of potential, which is described by the tilt of the bands. As mentioned in the introduction, the contact may be composed of some combination of materials, involving very thin metal oxides; that is why we refer more generally to electron selective contact (ESC) and hole selective contact (HSC).

Now we need to make an important distinction. We call V the voltage in the device, which is defined as the following quantity:

$$-qV = E_{\text{Fn}}(L) - E_{\text{Fp}}(0) \quad (1)$$

Here q is the positive elementary charge, E_{Fn} is the Fermi level of electrons, E_{Fp} is the Fermi level of holes, and L is the thickness of the layer. The voltage is the difference of Fermi levels at the contacts, and we use the assumptions that with (good) contacts, the Fermi level in the metal is the same as that at the correspondent edge of the organic layer. The voltage V can be varied with the power source,¹⁹ and by illumination, the solar cell produces a voltage that is called the photovoltage.

Another quantity of interest is the local *electrostatic potential*, φ . The variation of the potential is represented in Figure 1 by the variation of the bands. This idea can be put in more formal terms with the notion of the vacuum level,^{20,21} but here we do not use such explicit representation. We must clarify that Figure 1 provides, in general, a representation of electron energies, hence the voltage is converted to energy by product with $-q$. However, in Figure 1b we show for clarity the electrical potentials at the edges of the blend layer, and these correspond to a different scale that is shown at the right-hand side. This is because we need to discuss the relationship between the voltage and the variation of the potentials, which is an important feature of any model for the BHJ, since the electrical field F_{dr} at any point of the organic layer is given by the expression

$$F_{\text{dr}} = -\frac{\partial\varphi}{\partial x} \quad (2)$$

In Figure 1, the electrical field in the organic layer, which we call the *drift field* (to distinguish from possible electrical field at the contact) is constant and has the value

$$F_{\text{dr}} = -\Delta\varphi/L \quad (3)$$

where $\Delta\varphi$ is defined as the difference of potentials across the organic layer

$$\Delta_{\text{dr}}\varphi = \varphi(L) - \varphi(0) \quad (4)$$

Moreover, in the equilibrium situation (b), the energy difference of potentials at the boundaries of the layer coincides exactly with the original difference of work functions. Hence we introduce the built-in potential between the metals, which is the potential difference in equilibrium across the organic layer:

$$V_{\text{bi}}^{\text{a,c}} = \Delta_{\text{dr}}\varphi^{\text{eq}} = \varphi^{\text{eq}}(L) - \varphi^{\text{eq}}(0) = \frac{\phi_{\text{a}} - \phi_{\text{c}}}{q} \quad (5)$$

Note that $V_{\text{bi}}^{\text{a,c}}$ (which is >0 in Figure 1) coincides with the contact potential difference of the metals, and the organic layer has no role in determining $\Delta_{\text{dr}}\varphi^{\text{eq}}$.

To consider the changes of voltage, we first need to distinguish a *forward voltage*, that is, a negative voltage V applied to the ESC (or a positive voltage applied to the HSC), as shown in panel c, and the *reverse voltage*, defined as a positive voltage applied to the ESC as in panel d (or a negative voltage applied to the HSC). In general, the forward voltage facilitates injection toward the organic layer and increases the number of carriers, while the reverse bias voltage usually causes a situation of unfavorable energetics at the contacts and tends to remove the carriers from the semiconductor. Indeed, it should be recalled that the Fermi levels (often termed quasi-Fermi levels) are closely related with the number of carriers that are thermalized in the respective energy level.

The probability of occupancy of the energy level E , is given by the Fermi–Dirac distribution function $f(E - E_{\text{F}})$:

$$f(E - E_{\text{F}}) = \frac{1}{1 + e^{(E - E_{\text{F}})/k_{\text{B}}T}} \quad (6)$$

Here k_{B} is Boltzmann's constant, and T is the absolute temperature. For the occupation of the conduction band level we obtain

$$n = N_{\text{c}}f(E_{\text{c}} - E_{\text{Fn}}) \quad (7)$$

where n is the number density of electrons and N_{c} is an effective density of states (DOS). If the Fermi level of the electrons stays below the conduction band, so that $E_{\text{c}} - E_{\text{Fn}} \gg k_{\text{B}}T (= 0.026 \text{ eV at } 300 \text{ K})$, eqs 6 and 7 can be described by the Boltzmann distribution:

$$n = N_{\text{c}}e^{(E_{\text{Fn}} - E_{\text{c}})/k_{\text{B}}T} \quad (8)$$

The forward voltage has the effect that E_{Fn} approaches E_{c} , increasing the number of electrons, and similar well-known considerations and expressions can be given for hole carriers.

In Figure 1c,d,f we see a standard representation of the effect of the voltage in the BHJ. This figure is a suitable introduction of main concepts that uses the approximation of a constant electrical field in all situations, and the more general case is discussed later. By definition 1, the voltage creates a separation of Fermi levels of the contacts. The subsequent effect according to this model is that the tilt of the bands is reduced at forward bias and increased at reverse bias voltage. Consequently, the drift field decreases at forward bias and vanishes when the applied voltage equals the built-in potential, i.e., at $V_{\text{app}} = V_{\text{bi}}^{\text{a,c}}$. In this case, the bands are flat, and the applied voltage effectively restores the situation of Figure 1a. All the situations in Figure 1 are described by the following relationship:

$$\Delta_{\text{dr}}\varphi = V_{\text{bi}}^{\text{a,c}} + V_{\text{app}} \quad (9)$$

This result indicates that the applied voltage directly changes the drift field. However, it is important to recognize that such a picture of potential and field distribution is not a necessary consequence of the application of voltage. In reality, all the graphs of Figure 1 require an additional assumption, which is that *the distance between the Fermi level of the metal and the respective band edge in the organic layer at the contacts is independent of voltage*. However, it should be recognized that this boundary condition is very specific, and has the strong consequence that the density of the respective carrier is fixed at the boundary, by eq 8. For the purpose of clarity here we term this condition the *locked density boundary condition* (LDBC); we mean by this that the density of the carrier that is extracted at that boundary is fixed at the initial equilibrium level in all conditions.

To examine the consequences of LDBC on the behavior of the device, we also need to state what happens with the carrier that is *not* extracted at one boundary. Another common assumption in the literature of organic solar cells is that such a carrier should also remain at equilibrium level. Hence the contact is assumed to be a strong recombination center, and this boundary condition (sometimes stated in terms of surface recombination velocity) means that the less abundant (minority) carrier density at the contact is fixed at the equilibrium level in all conditions. A schematic view of this model that combines LDBC at both contacts is shown in Figure 2a. (Incidentally, it should also be noted that the abrupt drop of the Fermi level would imply a very

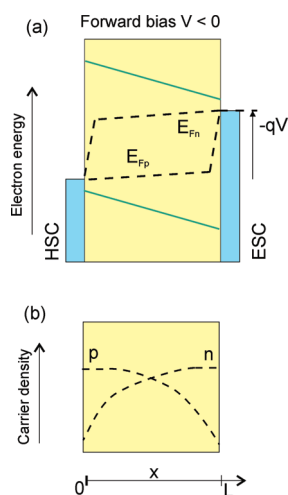


Figure 2. (a) Schematic representation of the bands and Fermi levels at forward bias voltage with the assumption of LDBCs. (b) The carrier distribution (electron and hole densities) in the organic layer.

short diffusion length.) Figure 2 is only an approximate representation of the device model that follows from the assumption of LDBC. In panel b we observe that a very specific distribution of carriers is obtained, which is very large at the extracting side and small at the opposite edge. This distribution of carriers is just the result of the boundary conditions.

Now the distribution of carriers can be considered in more detail. In fact, the electrical field in the organic layer is determined by the Poisson equation

$$\frac{\partial F}{\partial x} = \frac{\rho_e}{\varepsilon \varepsilon_0} \quad (10)$$

where ρ_e is the charge density per unit volume, ε is the dielectric constant of the medium, and $\varepsilon_0 = 8.85 \times 10^{-12} \text{ F m}^{-1}$ is the permittivity of the vacuum. Normally ρ_e consists of a combination of free carriers, trapped carriers, and ionic charge. Equation 10 shows another condition that is used in the standard diagram of Figure 1b. The straight bands mean that $\rho_e = 0$. This is a model for an insulator that contains no free charges. All the carriers that sustain the electrical field lie at the contacts.

For the reverse voltage situation of Figure 1b, it is reasonable to paint the straight bands, because the strong field withdraws all carriers from the sample, so the diagram is self-consistent.

At forward bias, it is required that the Fermi levels separate in the center of the device, and excess carriers must be created. To find the carrier and field distribution, a standard set of equations must be solved: this includes the continuity equation and drift-diffusion equation for each carrier, a statement of the recombination model, a statement about trap and transport states, and eq 10. Now the drift field is variable, and eq 3 is not true, but in general we have

$$\Delta_{\text{dr}}\varphi = - \int F_{\text{dr}} dx \quad (11)$$

In addition to the mentioned set of equations, in general it is necessary to fix the boundary conditions, and this has the essential role to determine the relationship between voltage and $\Delta_{\text{dr}}\varphi$. A widely used condition is given by eq 9, that now allows for a bending of the bands via eq 11. The bending of the bands is due to space-charge distribution created by the free carriers themselves.

Therefore Figure 1c,d, and Figure 2 are not accurate, because, in general, the use of the Poisson equation produces a moderate or strong bending of the bands at forward bias. However, these figures are still representative of many models in the literature because the essential feature governing these diagrams is the LDBC, which imposes eq 9. This means that any variation of voltage is automatically translated into a variation of $\Delta_{\text{dr}}\varphi$, and charge distributions such as those in Figure 2b appear as a result.

The Voltage-Dependent Density Boundary Condition (VDDBC). In this paper we emphasize that boundary conditions, which physically reflect the behavior of the carrier at the contacts, are a central element for the understanding the operation of solar cells and BHJ solar cells in particular. The essence of this view is that the polymer/fullerene BHJ solar cell works by kinetic selectivity, and we may dispense it with electrical fields. Kinetic selectivity occurs first at the nanoscale, producing electron hole separation in the two phases from the primary excitation. This gives rise to separate electron and hole Fermi levels, which is an incipient photovoltage. Kinetic selectivity must also exist at the contacts, then providing measurable photovoltage, and this also produces a unique direction for electron flow that creates the photocurrent.

One key point to clarify this view is to determine whether eq 9 and the LDBC are generally justified or are there other options. Note that this is a fundamental question that amounts to the definition of the voltage in the solar cell, which is one of the basic parameters that are measured. If eq 9 is not right, everything changes.

Equation 9 is used historically in the models of photoconductivity in insulators. For example, in the classical model of Goodman and Rose,²² the contacts are noninjecting for both electrons and holes; i.e., carriers can only be extracted from or flow out of the photoconductor into the contacts. Sokel and Hughes²³ model sets all carrier densities to zero at the boundary.

The LDBC finds application in problems of carrier injection in insulators, such as in organic light-emitting diodes (OLEDs). In these systems, current is driven by strong forward bias voltage to cause luminescence, and is usually a space-charge limited current (SCLC). The boundary conditions in SCLC-dominated systems pose some problems, because the carrier density increases without limit at the injecting contact. One solution is to assume that the number of carriers at the boundary is set to the limit of the local DOS, hence the LDBC is justified in this case.²⁴ It is also worth pointing out that the injection rate of carriers at the contact takes control of the device current at very high current levels or large applied voltages. Current becomes proportional to the applied voltage, and departs from the space-charge limitation.²⁵

It should be noticed that the main reason for the use of LDBC in the BHJ solar cell is the equilibrium picture of Figure 1. It appears that this figure is not obtained from the necessary physical principles but from a rather widespread belief that requires one to visualize an electrical field that will drive electrons and holes in separate directions as a requirement to obtain a photocurrent. Such a belief has been held for many years in the area of inorganic solar cells, where the *pn* junction is said to realize this function. In the BHJ area, the requirement of a drift field in the model is reinforced by the also widespread notion that an electrical field is needed to separate excitons into electron and hole carriers, a topic we comment on in more detail later on.

However, in general, solar cells do not require such an electrical field. This point is further commented on in the Supporting Information (SI), and has been explained in detail, for example,

on page 133 of Würfel's book.²⁶ The clearest case is the dye-sensitized solar cell, in which the electron–hole pair generated in a molecular absorber is rapidly separated into *n*- and *p*-type conducting materials by kinetic preference that depends to a large extent on relative positions of carrier energy levels.

The organic blend in a BHJ with a viable PCE must be a reasonably good conductor of electrons and holes. We must consider the possibility that such electrons and holes construct *separate* equilibration conditions to the anode and cathode. A large number of studies have addressed the formation of the metal–organic interface. This area is too broad and complex to attempt a minimal review here, and we refer to the literature.²⁷ It is shown that equilibration of the Fermi levels is obtained in a few molecular layers, often accompanied by a strong interaction of the organic molecules on the metal that produces a local dipole at the interface. This effective dipole layer is caused by any inhomogeneous distribution of the charge at the surface that may have diverse origins. As an example, surface reconstruction involves the outward or inward displacement of surface atoms, and electrostatic dipole layers are formed, which change the measured affinity. As a result, the barrier between the Fermi level of the metal and the lowest unoccupied molecular orbital (LUMO) of the organic can depart strongly from the original difference of work functions.²⁸ If separate equilibria occur at the two contacts, Figure 1b, that is, based on a global equilibration, is not justified. Interestingly, it has also been shown that, for organic solar cell devices formed by several doped layers, the built-in potential corresponds to the difference of Fermi levels of the doped layers rather than to the work function of the metal electrodes.²⁹

Electrons and holes construct *separate* equilibration conditions to the anode and cathode.

The next question we consider is the carrier density. We have mentioned that an electrical field is not a necessary requirement for photovoltaic energy conversion. What is necessary is a split of the Fermi levels. In fact, the effect of the light must be to create separate electrons and holes in the blended organic layer. The increased carrier density produces the separation of Fermi levels that drives the photocurrent and can be measured as a voltage in the outer contacts. Therefore, in a solar cell, the density of at least one carrier must significantly increase with respect to the equilibrium level. For example, if the electron density increases under illumination, the Fermi level of electrons approaches the conduction band (see eq 8). It is then rather unclear why this should not happen at the boundary as implied by LDBC.

A different view of the solar cell model that does not use the LDBC is shown in Figure 3. This is again a schematic model, but serves to introduce a number of important concepts. We start with a doped material that contains a density of holes as indicated by the equilibrium Fermi level E_{F0} being close to the valence band in panel a. After contact, both the hole selective layer and electron selective layer take the level of the equilibrium Fermi level. In the case of the hole selective material, this is a rather easy process because the energetics are similar before contacting.¹¹ In the case of the electron selective layer, it is evident that the

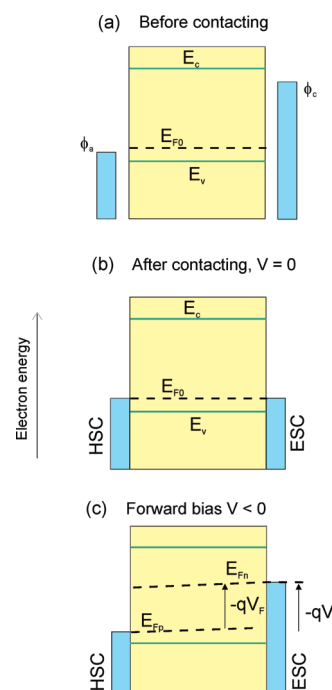


Figure 3. Schematic representation energy diagram of a *p*-type organic layer with an acceptor LUMO level for electrons E_c and a donor HOMO level for holes E_v and two contacts, an ESC with work function ϕ_c , and an HSC with work function ϕ_a . The contacts are considered to be metals in which the carrier energy level is at the Fermi level. The boundary conditions assume that the voltage produces a modification of the Fermi level of minority carriers (electrons) with respect to E_c at the left contact, while holes remain at equilibrium at the left contact. (a) The energies of the separate materials and (b,c) different situations of bias voltage V (q is elementary charge) indicating the Fermi levels of electrons (E_{Fn}) and holes (E_{Fp}).

original difference $E_{F0} - \phi_c$ must be absorbed by a potential drop at the interface.

The main question we need to discuss is the behavior of carrier densities and Fermi levels upon application of forward voltage. This is shown in Figure 3c. The basic effect of the voltage is to produce an increase of the minority carriers (electrons), raising their Fermi level. Note that E_{Fn} approaches the conduction band at the contact. In fact, the voltage V is invested totally in a separation of the Fermi levels (how deep the separation enters the layer depends on the recombination rate). Note the contrast of this condition with the LDBC. We term the condition of Figure 3c the VDDBC. This means that the potential applied in the ESC fixes the Fermi level of electrons and their density at the contact. We furthermore require that the contact is reversible, meaning that such an operation condition occurs either if voltage is applied or if electrons are placed at the organic surface. This is then a very desirable attribute for the operation of a solar cell. Upon illumination, the photogeneration creates a density of electrons at the contact and consequently fixes the Fermi level. The Fermi level at the ESC takes just this value and goes up providing photovoltage. This interface behaves as an ohmic contact for the electrons.

A VDDBC that equilibrates to the metal potential can be written with a simple quantitative expression that can be used as the boundary condition in modeling. Consider again the simple expression of the Boltzmann statistics with respect to the local

Fermi level (eq 8). In Figure 3 we have assumed an electrochemical equilibrium condition (b), hence we can set the equilibrium concentration of electrons as

$$n_0 = N_c e^{(E_{F0} - E_c)/k_B T} \quad (12)$$

Consequently, we write eq 8 as

$$n = n_0 e^{(E_{Fn} - E_{F0})/k_B T} \quad (13)$$

and the required boundary condition for Figure 3c is

$$n_s = n_0 e^{-qV/k_B T} \quad (14)$$

where n_s is the concentration at the boundary.

One should carefully note that V in eq 14 is not the total voltage applied in the device, but just the voltage that produces a separation of Fermi levels. We term this part of the total voltage V_F (to distinguish it from the potential drop at series resistance, for example).^{30,31}

Another point of interest is that the concentration of the carrier that is not extracted does not decrease abruptly at the interface. This allows for the Fermi level to be nearly horizontal in cases in which the diffusion length is long. Holes are simply blocked at the right boundary and electrons at the left boundary. This is called a reflecting boundary condition and is represented in models by the condition that the current of the reflected carrier is zero at the boundary. The current due to electrons can be expressed in terms of the fundamental equation³²

$$j_n = -nu_n \frac{\partial E_{Fn}}{\partial x} \quad (15)$$

where u_n is the mobility. Hence the reflecting boundary condition requires that the Fermi level is horizontal at the boundary. By this condition, the density of the blocked carrier is also variable at the boundary, for example, the electron concentration may increase and become large provided that $\partial E_{Fn}/\partial x = 0$.

What is the physical condition of material properties that serve to form a VDDBC whereby electron density reversibly equilibrates with the (variable) potential at the cathode? Above we mentioned kinetic selectivity, which is in part determined by the energetic levels of the materials, but we must recognize that it is difficult to specify those kinetic processes that are in many cases determined empirically. In general, the physics of the metal/organic semiconductor interface is poorly understood. Empirical investigation of different contacts at high injection conditions indicates that minimizing the energy barrier to one carrier helps make a contact ohmic to that carrier at a metal/organic semiconductor interface.^{25,33} It is thus natural to use a low work function material as the cathode on the right of Figure 3a. In equilibrium, we require the cathode potential to go down a large fraction of a volt, as shown in Figure 3b. When a sizable electron density occurs in the blend, by photogeneration, the cathode material will take the value of the Fermi level of electrons in the organic semiconductor and will go up as in Figure 3c, if eq 14 is satisfied.

It is interesting to point out that cells, providing high $V_{oc} = 1$ V, with appropriate electron and hole selective contacts, have been constructed, having no initial difference of work function between the metals, i.e., with $V_{bi}^{a,c} = 0$.³⁴

In Figure 4 we draw a more elaborated model that takes into account the role of the intrinsic carriers in the organic blend for the establishment of equilibrium. Now the potential drop required to bring the cathode level down is partially accommodated

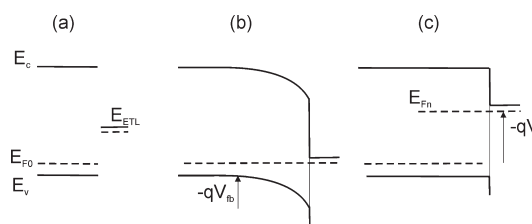


Figure 4. Schematic representation energy diagram of a *p*-type organic layer and ESC as the contact for the device. (a) The separate materials. (b) In contact, the original difference of work functions is divided between a depletion zone at the organic layer with barrier V_{fb} and an interfacial dipole. (c) When the flatband potential is overcome by negative potential or by photogeneration of electrons, the electron density at the surface increases.

in the organic. A depletion layer is formed at the surface, and the band is not flat because it corresponds to the solution of eq 10 with $\rho_e = -qN_A$, with N_A being the immobile defect acceptor density. As is well-known, the solution is parabolic, and the resulting structure is a Schottky barrier. The height of the barrier, which is the flatband potential, is given by the difference of the Fermi level of the blend, $\phi_s = E_{F0}$, and the cathode work function

$$V_{fb} = V_{bi}^{blend,c} = [E_{F0} - \phi_c]/q \quad (16)$$

as shown in Figure 4b. Polarization of the junction first removes the barrier, and at further negative potential the density of electrons rises at the surface as in Figure 3 according to the expression

$$n_s = n_0 e^{-q(V - V_{fb})/k_B T} \quad (17)$$

It is assumed that no (accumulation) band bending is formed close to the cathode contact after the flatband condition, since the fullerene network is able to redistribute the electron carriers.

We point out that Figure 4b also indicates the role of a *pn* junction that is used at the boundary as a selective contact in an efficient *p*-doped monocrystalline silicon solar cell.³⁵ In a dye-sensitized solar cell, the contact corresponding to Figure 4 is a contact between nanostructured TiO_2 and the transparent conducting oxide. It is well established that the band bending is rather narrow, a few nanometers thick,³⁶ hence such band bending is often skipped in diagrams, and Figure 3 is also a good representation of a DSC. Further discussion of these photovoltaic devices is provided in the SI.

Turning our attention to the BHJ, it would be useful to establish a general rule like eq 16 so that the energetics of the junction, and the subsequent selective properties and ohmic behavior at forward bias, could be determined from separate properties of the constituent materials that come into contact. However, in contrast to the silicon *pn* junction, the contact of the BHJ is a heterojunction. In addition, the studies of metal/organic junctions^{25,28} show that this type of contact is extremely sensitive to deposition conditions, impurities, and so on, and furthermore the contacts are often formed by a combination of materials and/or layers to improve ohmicity and selectivity.³⁷ These effects imply that eq 16 is modified to the more general expression

$$V_{fb} = [E_{F0} - \phi_c - \Delta_i]/q \quad (18)$$

where Δ_i is the interfacial dipole that accommodates part of the potential drop. In situ measurement of the junctions of the BHJ devices seems to be required, as we discuss in the following.

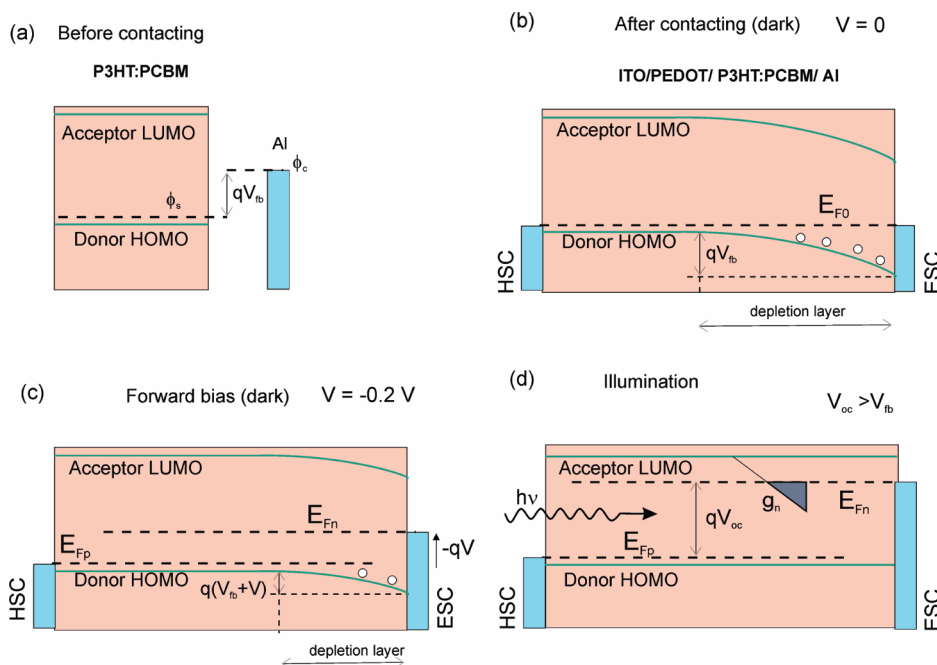


Figure 5. Band structure of the P3HT:PCBM heterojunction. (a) Separate representation of the blend and the cathode metal. (b) Equilibrium after contact ($V_{\text{app}} = 0$). Band bending appears near the cathode (ESC), and holes can occupy HOMO states of the P3HT within the neutral region. (c) Forward voltage lower than the flatband condition at the cathode. (d) Open circuit condition under illumination.

Carrier Distribution Based on Capacitance Measurements. We have discussed two rather different views of the operation of BHJ solar cells. We have identified that the physics of contacts and the nature of the blend layer as an insulator or doped semiconductor lead to very different pictures. What is at stake here is not only the detail of boundary conditions to use in modeling, but rather the role of the voltage and which aspects are critical for the operation mechanism of BHJ solar cells. Clearly, the model of Figure 1 relies on investing the voltage in the potential difference that controls the drift electrical field. This model emphasizes exciton dissociation as a predominant effect in the current–potential curves of BHJ solar cells.

On the other hand, the model of Figure 3 denies eq 9 ($\Delta_{\text{dr}}\phi$ is not determined by the voltage; we can even have $\Delta_{\text{dr}}\phi = 0$). We claim therefore that BHJ solar cells, at least with the paradigmatic combinations of materials most studied so far, work by the separation of electron and hole carriers across the layer with appropriate selective contacts at the edges of the layer, in an operation model that is basically similar to crystalline silicon solar cells and dye-sensitized solar cells. However, the specific mechanisms of selectivity at the minority carrier contact are indeed quite different between these classes of solar cells. The model of Figure 4 accommodates part of the interfacial potential difference in a Schottky barrier. Understanding the properties of the cathode contact appears to be a challenging aspect of the BHJ research.

At this point it should be remarked that it is fair to ask authors of future papers on BHJ to really define what they mean by the applied voltage, as eq 9 is not a universal requirement.

The question arises how to establish which model should be used in BHJ modeling and discussion. One important problem to answer this question is the great number of parameters involved in a realistic modeling, consisting of the dozen or so equations mentioned above. The difficulty here is that very different models could all equally fit a series of current–potential curves.

To address this question, we have, in recent work, employed another technique that is not so versatile with respect to models. Measurement of impedance spectroscopy (IS) allows resolving the capacitances and resistances in the solar cell when the device is set at a certain condition of bias voltage and illumination. The capacitance, if properly interpreted, is an excellent tool to provide information about carrier distribution.

Here we do not repeat the experimental evidence that is already summarized in previous papers; however, some representative data are shown in the SI. We just describe in Figure 5 a model of the internal behavior of P3HT:PCBM BHJ that arises from the mentioned studies. We refer the reader to the original papers for the justification of this model.^{15,31,38}

Figure 5a shows a central property of the polymer/fullerene blend. The equilibrium Fermi level of electrons and holes is shown close to the HOMO level of P3HT, and this means, as stressed in Figures 3 and 4, that from the beginning we assume that the blend is not an insulator; rather it contains hole majority carriers, with characteristic densities (in our measurements) of 10^{15} – 10^{17} cm^{-3} , which is a significant concentration, as the photogenerated carrier density at 1 sun can barely exceed these numbers. The origin of these majority carriers are negatively charged defects that cause *p*-doping of P3HT when exposed to the air or moisture,^{39,40} or structural defects induced during blend processing.⁴¹ The evidence for the *p*-doped behavior arises from the observation of Mott–Schottky (MS) lines ($C^{-2} \propto V$) in the capacitance of most samples that have been measured.^{15,31,38,42–44}

In Figure 5b, we indicate that when the blend is contacted with the electron extracting contact of low work function ϕ_c , a Schottky barrier is formed at this contact. This is the mechanism already explained in Figure 4. A depletion zone at the blend/ESC contact is formed, which entails bending of the transporting bands. The width of depletion zone obviously depends on the layer thickness and the doping level, but since the thickness of

polymer/fullerene BHJs is on the order of 100 nm, the depletion zone can occupy a significant portion of the active layer. On the other hand, the anode contact is regarded as an ohmic contact because of the practical alignment between the PEDOT:PSS HSC at the contact and P3HT HOMO levels.

The previous explanation on the formation of a depletion zone implies that the active layer will be split into two regions: near the cathode, band bending removes the majority carriers out from the depletion zone, the rest forming a neutral zone.⁴⁴ Defect acceptors make up a space-charge region of immobile charges in the depletion zone, while their charge is compensated by mobile majorities in the neutral zone. A sharp spatial step for hole density between N_A (neutral zone) and zero (depletion zone) does not exist in reality. In practical terms, a smooth spatial change occurs, which is related to the ability of mobile charges to screen the electrical field. The Debye length gives the spatial distance needed for an effective field screening. Assuming Boltzmann statistics, the Debye length decreases with increasing concentration of carriers (mobile holes for the p -doped active layer) as

$$\lambda_D = \left[\frac{\epsilon \epsilon_0 k_B T}{N_A q^2} \right]^{1/2} \quad (19)$$

Most doping levels usually encountered lie within the range of 10^{16} – 10^{17} cm⁻³, so that one can find that λ_D ranges from approximately 20 nm down to 6 nm at 300 K, assuming $\epsilon \approx 3$ for organic compounds. This last observation implies that charge carriers present in dark conditions suffice to screen macroscopic fields within neutral regions.

Now we discuss the effect of the applied voltage. At forward bias, there are two different voltage ranges. First moderate forward bias polarizes the Schottky barrier as in standard diodes (see, for example, the paper by Green et al.⁴⁵ that depicts exactly the same type of barrier). The band bending decreases toward the cathode contact (see panel c). At $V = -V_{fb}$ (flat-band conditions), which is about $V_{fb} = 0.3 - 0.5$ V, the depletion layer adjacent to the P3HT:PCBM/M contact disappears, and the neutral, doped region extends along the whole bulk of the organic layer. The flatband potential can be determined accurately by the intercept of the MS plot.

When the forward voltage progresses beyond the flatband condition, we find that the behavior of the capacitance changes and shows a chemical capacitance⁴⁶ that records the DOS of electrons in the PCBM (see eq 20 below).^{47,48} This capacitance has been obtained by measuring the solar cell under illumination at V_{oc} (see Figure 4d). Here the Fermi level of electrons rises homogeneously, and also at the contact, as stated before in VDDBC, approaching the LUMO of the PCBM. (By contrast, in a pn junction, the condition $V = V_{fb}$ removes the contact selectivity, and the photovoltage cannot exceed this value.)

Finally, if a reverse voltage is applied, then all the carriers are removed from the blend region, which becomes a dielectric, and in this case there is an overall drift electrical field. This is well described by Figure 1e, and confirmed by the stabilization of capacitance versus voltage to the constant value of the dielectric capacitance of the blend (see the SI).

In conclusion, this model proposes that the initial $\Delta_{dr}\varphi^{eq}$ consists of the V_{fb} indicated in eq 18. We remark that this $\Delta_{dr}\varphi^{eq}$ is associated with $V_{bi}^{blend,c}$, and not with $V_{bi}^{a,c}$. Each contact has its own equilibration, due to the starting number of electronic carriers

in the blend. The initial $\Delta_{dr}\varphi$ is reduced by the applied forward voltage. For the forward bias past the flatband of the cathode, we suggest the simplest model consistent with the observed behavior of the capacitance. Transport of either electrons and holes has not yet been extensively studied by IS at forward bias, and some comments on this are given in the SI.

Density of States. Starting from the range of properties discussed previously, we now focus on the most important features of the P3HT:PCBM BHJ concerning the photovoltaic performance. We start our discussion with the behavior of the capacitance at voltages more negative than $-V_{fb}$, as this is close to the operating point of the solar cell. We have mentioned above that in this domain of voltage we observe a chemical capacitance, which has the expression^{46,49} (per unit volume)

$$C_\mu = q^2 \frac{\partial n}{\partial E_{Fn}} \quad (20)$$

If there are abundant trap states that produce a density of localized electrons n_L , distributed in the DOS in the bandgap $g_n(E)$, we must write

$$n_L = \int_{E_v}^{E_c} n_L(E) dE \quad (21)$$

where

$$n_L(E) = g_n(E) f(E - E_{Fn}) \quad (22)$$

is the number of thermalized carriers at the energy level E . In the approximation that the occupation of electrons in localized states begins sharply at the Fermi level (and is zero above), the chemical capacitance gets a very simple expression:^{46,49}

$$C_\mu^{trap}(E) = q^2 \frac{\partial n_L}{\partial E_{Fn}} = q g_n(E_{Fn}) \quad (23)$$

We thus obtain that the capacitance spectroscopy directly records the DOS of electrons in the fullerene at the Fermi level. This result is obtained by our IS measurements^{47,48} and by other groups that use different experimental approaches to the chemical capacitance.^{50,51} Some authors prefer to plot the total charge density $n(V)$, which is obtained by integration of the differential in eq 23, which is the measured quantity. However, integration to derive an average number of carriers in the organic layer is only justified if the measured differential capacitance is indeed a chemical capacitance (while not if the capacitance lies in the domain of the Schottky barrier). This is also the reason why the lifetime is not meaningful at low voltage.⁵⁰

According to our previous discussion, we interpret that the measurement of the capacitance scans the DOS in the fullerene, and Figure 6 provides a representation of this model, showing realistic HOMO and LUMO levels of both polymer and PCBM,^{52,53} the measured distribution of localized states in the PCBM, as well as a distribution of localized states that should be present in the polymer. The LUMO in the PCBM, as well as the HOMO in the p -type polymer, are quantities that can be measured by electrochemical methods, and these energy levels are identified with reduction and oxidation peaks of the molecular materials. The bandgap can be determined by optical absorption, by the onset of photoexcitation of the material as indicated by process 1 in Figure 6. Then the measurement of the capacitance views the localized states in the bandgap, and one could assume that the measured DOS is a prolongation of a broadened LUMO of the fullerene. It is appropriate to assume a

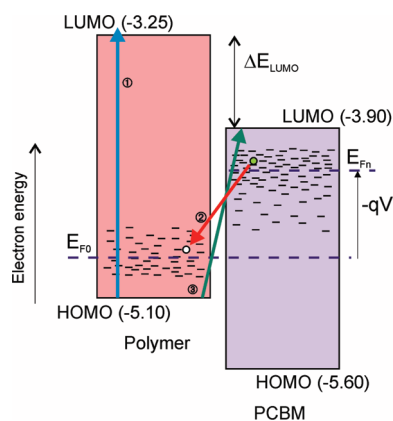


Figure 6. Approximate energy diagram of the P3HT:PCBM heterojunction indicating the trap states in the bandgap of both materials, the equilibrium Fermi level (E_{F0}), and the electron Fermi level at 1 sun illumination (E_{Fn}). The arrows show the following processes: (1) primary photoexcitation of the polymer across the bandgap, $h\nu = 1.85$ eV; (2) recombination of an electron in PCBM close to the Fermi level, to a hole close to the Fermi level in the polymer; and (3) photoexcitation of an electron close to the HOMO of the polymer, to a localized state close to the LUMO of the PCBM, $h\nu = 1.20$ eV.

Gaussian distribution of states,⁴⁸ and this assumption allows one to explain well the observed property⁵⁴ that open-circuit voltage in a BHJ solar cell is always less than the “electrical gap” $E_{LUMO,PCBM} - E_{HOMO,polymer}$.^{54–56} Recent measurements including the interfacial dipole at the organic/organic interface indicate that the gap of the PCBM:P3HT blend is ~ 1.4 eV, while $V_{oc} \approx 0.6$ eV.⁵⁷

The existence of a broad DOS is a general feature of disordered organic semiconductors.^{32,58} The determination of the DOS of the fullerene provides results that can be interpreted as an exponential distribution or as the tail of a Gaussian: both models are not easy to distinguish.⁵⁹ In any case, it is well established that $g_{PCBM}(E)$ raises exponentially from E_{F0} to E_{Fn} at the highest V_{oc} values recorded at 1 sun, and this physical property is suggested by the density of localized states depicted in Figure 6 and is shown in Figure 7a. The MS feature mentioned above provides a determination of the doping properties of the blend. This enables us to distinguish whether variations of photovoltage between different solar cells are due to changes of the equilibrium Fermi level, E_{F0} , which is our essential reference in measurements of the photovoltage,¹⁵ or to the properties of the DOS.⁴⁷

The analysis of energetics provides the fundamental background to discuss the kinetic properties of the BHJ solar cell. The usual view, held by many (but not all) researchers in this field, focuses on individual events starting from the photon absorption event. An exciton, generated in the polymer, diffuses to the interface, undergoes dissociation, forms a charge transfer bound state (CTBS), consisting of a bound electron–hole pair of the carriers in the separate materials; finally the CTBS dissociates and hence the photocurrent is obtained. These ideas have launched an enormous quantity of research on spectroscopies of the primary and transient photoexcitation involving the excitons.⁶⁰

In contrast to this, our approach focuses on the Fermi levels of the separate carriers. The Fermi level (or quasi-Fermi level) is a collective property of the carriers and is strongly influenced by the disorder in the material. Our view is clearly expressed in eq 1

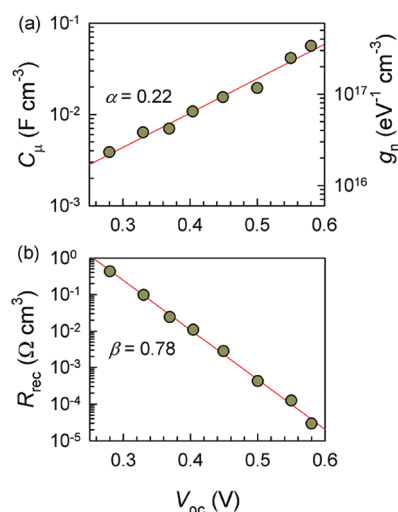


Figure 7. (a) Chemical capacitance extracted from IS of a P3HT:PCBM-based solar cell, exhibiting an exponential dependence on V_{oc} as $C_{\mu} \propto \exp(\alpha_q V_{oc}/k_B T)$ with $\alpha = 0.22$. If an exponential tail of trapping states is assumed to be $g_n(E) \propto \exp(E/k_B T_0)$, then $\alpha = T/T_0$, with T_0 being the characteristic temperature of the exponential distribution. (b) Recombination resistance following $R_{rec} \propto \exp(-\beta q V_{oc}/k_B T)$, with $\beta = 0.78$.

and proposes that the voltage is the difference of the Fermi levels at the contacts. This is otherwise well-known and widely accepted. To simplify the discussion, let us consider $E_{FP} = E_{FO}$ fixed. Then the photovoltage depends on the number of electrons created by the light. These electrons producing the photovoltage are expressed in eqs 20 and 21. The electrons fill the DOS from below. So these are not “free electrons” (or polarons) as they lie in localized, trap states. So which electrons contribute to the photovoltage? To answer this, we must turn to the meaning of the Fermi level, which is calculated using Fermi–Dirac statistics. The Fermi level (electrochemical potential) depends on the energy of the carriers but also has an entropic term that is the chemical potential. This means that electrons contributing to the Fermi level can be in any of the available states in the distribution. There must, therefore, be an easy communication between the states that we count in the DOS. This can occur by exchange with a common transport energy level, or simply by hopping between localized states.³² Therefore we define quasi-free electrons as those that can be exchanged rapidly between the distribution and hence determine the Fermi level that is measured from the outside. Strongly bound states of the electrons, which render them immobile, exclude those electrons from the ensemble that create the Fermi level.

We define quasi-free electrons as those that can be exchanged rapidly between the distribution and hence determine the Fermi level that is measured from the outside.

The photovoltage will be high if the rate of photogeneration is large, and if recombination of electrons is low. In addition, the

photovoltage depends on the DOS. If the DOS is small in a certain range of energies, the photovoltage rises fast.⁴⁷ Hence the chemical capacitance in eq 20 is an important property determining V_{oc} . If C_{μ} is very large, increasing the number of electrons can be accommodated with little change of E_{Fn} . This is what happens in a metal, in which the Fermi level is attached to one energy level, as mentioned before.

In our model of the solar cell, explained schematically in Figure 3 and in more physical detail in Figure 6, the photocurrent is created by gradients of the Fermi levels (see eq 15). A discussion on the detailed transport mechanisms in the polymer/fullerene blends is beyond the scope of this paper, considering, for example, the transport in the presence of the broad distribution of states in the energy space. However, the intuitive idea is that accumulated electrons and holes find an easy way out in the selective contacts. Of course this process is competing with recombination, which is the essential process we need to discuss.

Recombination. In this approach, which gives predominance to the measured quantities determining the solar cell performance, it is important to formulate the balance of carriers that ultimately produces the current density–voltage characteristics. To describe the current density–voltage curve of a BHJ solar cell, we may then use a simple model⁶¹

$$j = j_{sc} - j_{rec}(V) + j_{eq} \quad (24)$$

This model is based on the ideal diode structure of Figure 3.³¹ j_{sc} is the photocurrent, j_{eq} is a thermal generation term (that becomes irrelevant at moderate forward voltage), and $j_{rec}(V)$ is the recombination current. We emphasize that in eq 24, recombination is attributed to quasifree electrons and holes: those that produce the Fermi levels. Any other recombination mechanism (i.e., geminate recombination of the CTBS) is included in the generation term implicit in j_{sc} in eq 24, as discussed later. The central element of this model is to determine the physical basis for the recombination term, $j_{sc}(V)$, a point that has been emphasized in some recent papers.^{50,56,62,63}

According to the approximation of Figure 3, which takes homogeneous Fermi levels, the recombination current density is given by the expression⁴⁸

$$j_{rec} = qL \int \int g_n(E_n) f(E_n - E_{Fn}) g_p(E_p) [1 - f(E_p - E_{Fp})] \times \nu_{rec}(E_n, E_{Fn}, E_p, E_{Fp}) dE_n dE_p \quad (25)$$

This equation is directly derived from the energetic model of Figure 6. It is a count of the thermalized electrons and the thermalized holes in their respective DOS, and the probability for charge transfer from one kind of carrier to the other one. This is given by ν_{rec} , the probability of charge-transfer events at the organic/organic interface, i.e., for an electron at energy level E_n to recombine with a hole at energy level E_p , which is shown as process 2 in Figure 6. Equation 25 shows, more generally, the challenging complexity of recombination in the organic blend, which depends on the specific DOS in both the polymer and fullerene, their occupancy, and also on the charge transfer model represented by ν_{rec} which may consist, for example, of the Marcus model.^{48,64–66}

Equation 25 is a generalized bimolecular or nongeminate form (in the usual terminologies that we have been avoiding here) to the recombination process, which in its simpler version is usually

written as $j_{rec} = qLk_{rec}np$, with k_{rec} being the macroscopic recombination rate, and $n(p)$ being the total density of electrons (holes).

Fortunately, we have some experimental information on the recombination term of eq 24. Let us introduce the recombination resistance^{31,67}

$$R_{rec} = \frac{1}{A} \left(\frac{\partial j_{rec}}{\partial V} \right)^{-1} \quad (26)$$

where A is the device area. R_{rec} is a derivative of the recombination flux and is measured directly by IS, separate from series resistance contributions that heavily distort the voltage dependence.^{15,47,48,68} Representative results obtained so far in P3HT:PCBM solar cells are shown in Figure 7b, and allow one to write a very simple expression.

$$R_{rec}(V) = R_0 \exp \left[-\frac{q\beta V}{k_B T} \right] \quad (27)$$

Here β is a constant recombination parameter. By integration of R_{rec} in eq 27, we directly show the empirical expression of the recombination flux

$$j_{rec}(V) = j_0 e^{q\beta V/k_B T} \quad (28)$$

Here, j_0 is a constant equal to the “dark current” j_{eq} in eq 24, and it follows that

$$j(V) = j_{sc} - j_0 (e^{q\beta V/k_B T} - 1) \quad (29)$$

Hence we obtain the standard diode equation, and it follows that the recombination parameter β is the reciprocal of the diode quality factor.

The main point to explain the current–voltage curve is to understand the origin of the recombination term, both the prefactor j_0 that gives the total rate, and β that determines the voltage dependence and consequently the fill factor,^{31,69} in terms of a mechanistic model as Figure 6 and eq 25.

Equation 28 is useful as a first approximation to illustrate some measured properties of the recombination, but it is also an oversimplification of eq 25. In fact there is an open issue regarding the underlying physics of recombination: Can the recombination current be solely expressed in terms of the voltage, or is information on the carrier density profile absolutely necessary? This question relates to fundamental reciprocity arguments by which carrier density is univocally determined by the voltage, regardless of the irradiation intensity.^{70,71} One approach to address it may consist of analyzing whether the illuminated solar cell performance is related to the carrier concentration present in the same device under forward voltage in the dark. Further investigation of the dependencies of j_{rec} is then a key requirement to explain well the performance of this type of solar cells.⁷²

The Photocurrent. Finally, we turn our attention to the discussion of the photocurrent term in eq 24. We have adopted the assumption that, once separated, electrons and holes contribute to the photocurrent. This requires fast transport, an assumption that can be relaxed in more advanced models that incorporate the roles of mobilities and morphology. Hence j_{sc} depends basically on the ability of the blend to produce carriers. Under illumination with a source of photon flux ϕ_{ph}^{source} (in m^{-2}) we have

$$j_{sc} = q \int_{\lambda_{min}}^{\lambda_{max}} \eta_{EQE}(\lambda) \phi_{ph}^{source}(\lambda) d\lambda \quad (30)$$

where η_{EQE} is the external quantum efficiency (EQE), and λ_{min} and λ_{max} are the wavelengths where the EQE vanishes.

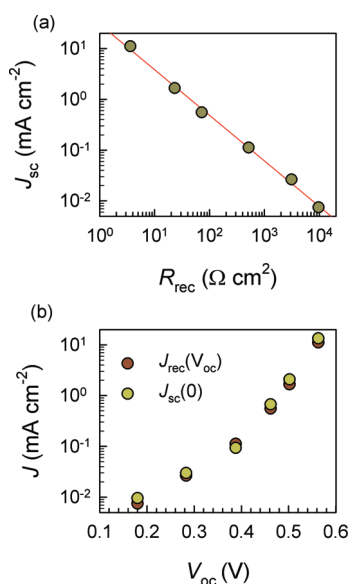


Figure 8. (a) Correlation between the short-circuit current j_{sc} and the recombination resistance $R_{rec}(V_{oc})$, extracted from IS at open-circuit conditions at different continuous irradiation levels, and (b) comparison of j_{sc} and $j_{rec}(V_{oc}) = j_0 e^{q\beta V_{oc}/k_B T}$ as a function V_{oc} of a standard P3HT:PCBM-based solar cell.

Neglecting factors such as the transmittance of the glass,⁷³ $\eta_{EQE}(\lambda)$ must depend on the absorption coefficient of the absorber material α_{abs} and the efficiency of charge separation of the blend, hence

$$\eta_{EQE} = \eta_{sep}(\lambda)\alpha_{abs}(\lambda) \quad (31)$$

The detailed physical picture leading from photon absorption to photocurrent is far from clear. First we note that cells of very high internal quantum yield have been demonstrated,⁴ in this case $\eta_{sep} \approx 1$, and we should look at recombination to improve such cells. Another question that has been widely debated is the dependence of η_{sep} on external variables such as the electrical field. This means that eqs 24 and 29 are not complete because of an additional dependence $j_{sc}(V)$ so that the fill factor is determined by $\eta_{sep}(V)$ as well as the recombination flux in eq 28.^{17,74} Recently it has been shown that in some P3HT:fullerene cells the photocurrent can be correlated with ΔE_{LUMO} (see Figure 6).⁷⁵ This implies that charge separation is determined by an interfacial energetic driving force that does not require a dependence of η_{sep} on external voltage.

A correlation between recombination current and the corresponding photocurrent has been shown before,⁷⁶ and here we present in Figure 8 new evidence that also points in the same direction. We highlight in Figure 8a the correlation between j_{sc} and $R_{rec}(V_{oc})$, as suggested by eq 29 in the case of a constant, voltage-independent photogeneration current, which is entirely balanced by the recombination flux in such a way that $j_{dc} = 0$. Interestingly, it is noted in Figure 8b that the photocurrent measured at short-circuit at different illumination intensities equals the recombination current calculated from the recombination resistance analysis at open-circuit, i.e.,

$$j_{sc}(V = 0) \approx j_{rec}(V_{oc}) = j_0 e^{q\beta V_{oc}/k_B T} \quad (32)$$

We observe in Figure 8a that j_{sc} varies by more than three orders of magnitude, for V_{oc} ranging within 0.2–0.6 V. The photogeneration flux is completely cancelled by the recombination current at open circuit within this voltage range. Consequently photogeneration can hardly be influenced by the voltage. More specifically, if η_{sep} , and consequently photogeneration, changes with the electrical field through the applied potential, being largely less than unity at bias approaching V_{oc} , one would expect that $j_{rec}(V_{oc}) < j_{sc}(V = 0)$, in opposition to the correlation in Figure 8b. It should be noted here that differences always less than 20% between $j_{sc}(V = 0)$ and $j_{rec}(V_{oc})$ are observed which might be related to the simplified diode equation used (eq 29) that does not consider the series resistance effect. Another important question is whether eq 28 is a good parametrization for carrier recombination. Parameters β and j_0 that state the recombination current might well vary with the irradiation intensity, signaling a light-induced change in the underlying recombination mechanisms. As commented upon above, this issue is a matter of further experimental research in relation to reciprocity theorems.

Role of Excitons in the BHJ Solar Cell Performance. We finish our analysis by speculating on the effect that quasi-free carriers might have on the physical factors governing η_{sep} . These considerations are not based on specific experimental evidence but on general physical properties of semiconductor devices, and aim to point out directions of research in BHJ solar cells. Clear evidence of excitonic effects in BHJ are not so apparent, and there is a question as to whether this type of solar cell is not so “excitonic” as widely thought, so that additional factors related to quasi-free electrons and holes must be a priority of investigation.

The usual understanding of processes immediately after generation is that necessarily an exciton is formed, which requires diffusing to the interface. However, recently it was pointed out that the exciton diffusion is too slow to account for the observed electron transfer rate.⁷⁷ In addition, it is often supposed that the exciton at the interface evolves into a CTBS, which then either recombines to the ground state or dissociates into quasi-free carriers via the manifold of charge-separated states.^{3,78,79} The evidence for CTBS has been mainly derived from

- Long wavelength absorption in the blend that is absent in the pristine material.^{80,81} Those optical transitions at the infrared, usually observed for excitation energies of $h\nu = 1.1$ – 1.2 eV, may well be also attributed to quasi-free carrier band-to-band-like absorptions. This is indicated in process 3 of Figure 6, and lower transitions are also possible due to the broadened DOS.
- Different rate of charge generation in sets of polymer blends for which photoluminescence quenching is similar.⁸²

The standard approach attaches great weight on the stability of the exciton due to both long-range of the Coulomb interaction and low dielectric constant, but the effect of a large ensemble of quasi-free carriers has been neglected in such a view.

As introduced previously in the analysis of the depletion layer (eq 19) quasi-free carriers have the ability of screening electrical fields. Strong shielding of the Coulomb interaction is then expected,^{83–85} which becomes a Yukawa potential governed by the inverse (Debye) screening length⁸⁶

$$\kappa = \left[\frac{q^2}{\epsilon \epsilon_0} \frac{\partial n}{\partial E_{Fn}} \right]^{1/2} \quad (33)$$

As mentioned in eq 19, for the Boltzmann statistics, the Debye length decreases with increasing concentration of carriers:

$$\lambda_D = \kappa^{-1} = \left[\frac{\epsilon \epsilon_0 k_B T}{n q^2} \right]^{1/2} \quad (34)$$

More generally, the inverse screening length (eq 33) correlates with the chemical capacitance:

$$\kappa = \left[\frac{C_\mu}{\epsilon \epsilon_0} \right]^{1/2} \quad (35)$$

The presence of quasi-free carriers might have, therefore, a strong influence on the rate of exciton dissociation. Simple arguments based on Debye–Hückel theory show⁸⁴ that the exciton binding energy decreases strongly at concentrations of $n \approx 10^{17} \text{ cm}^{-3}$, which is the carrier density that we found under steady-state illumination in several BHJ solar cells. Indeed, in a crude estimate, we find that if the spatial extent of the exciton is $d = 10 \text{ nm}$, then one quasi-free carrier is found in the sphere of the exciton if the density of carriers is larger than $n_c = [\pi(d/2)^3]^{-1} \approx 10^{17} \text{ cm}^{-3}$. This means that whenever a photon is absorbed, a quasi-free hole is there to shield the electron–hole interaction. If the carriers forming an exciton are strongly delocalized,⁸⁷ shielding will be more effective.

It is worth noticing here that the role of partial charges, which exist prior to photoexcitation, on increasing the dissociation yield of CTBS was analyzed previously.⁸⁸ In that work the effect of dipoles at the donor/acceptor interface was proposed to facilitate exciton dissociation. On the basis of this idea, exciton dissociation probability becomes electrical field independent for the usual dipole strength values as inferred from recent modeling.⁸⁹ Therefore, the presence of neighboring charges (either quasi-free carriers, interface dipoles, or charged defects responsible for the polymer doping) largely alter the simplistic image of an isolated electron–hole strongly bounded pair, and allows for an efficient exciton dissociation via a modified electrostatic landscape.

We must also consider additional factors that may contribute to improve the lifetime of separated states. In the end, efficient operation of BHJ solar cells requires that electrons (a) are transferred rapidly to the electron conductor and (b) do not return easily to the light absorbing polymer. So far fullerenes have shown unsurpassed ability to carry out these functions. Is there something special about the fullerenes that facilitates ultrafast charge separation and retains the electron over long distances? One should consider a process in which the network of fullerene molecules relaxes electronically when receiving electrons, inhibiting the reverse charge transfer process of the electron to the polymer, while maintaining electronic conductivity. Electrochemical results^{90,91} on clusters of fullerene derivatives showed that the cluster network exhibits better charge stabilization properties than the monomeric form. Recently, it was furthermore found that the aggregation of PCBM molecules under long time annealing has a positive impact on the fill factor of the BHJ solar cell.⁹² Further studies considering charge stabilization and shielding in BHJ blends seem necessary to clarify these effects.

In conclusion, we have suggested critical insights on the device physics of BHJ organic solar cells. In contrast to most approaches that start from the formation and separation of excitons, here we invert the priority of the analysis as we aim to follow the quantities

that are measured at the contacts and govern the power production of the solar cell. We have identified that the physics of the contacts and the nature of the blend layer as insulator or doped semiconductor lead to very different pictures. To give up the constraining view that the role of the electrical field imposes upon solar cell photocurrent and photovoltage, more flexible boundary conditions at the contact cathode are introduced. Charge separation and charge transportation have very little to do with built-in electrical fields, while kinetics plays a major role in photocurrent production. Electron density reversibly equilibrates with the (variable) potential at the cathode. Voltage-dependent carrier density boundary conditions allow for a dynamic alignment of the electron Fermi level and the cathode work function, giving rise to the output photovoltage. The effect of the applied voltage on the device electrical response is contrasted with the measurement of the differential capacitance. The *p*-doped character of the active blend is observed, which produces the formation of a majority carrier (holes) depletion zone in the vicinity of the cathode contact. MS analysis derived from capacitance–voltage measurements allows determining both the doping density and the equilibrium Fermi level position, which acts as an energy reference for the photovoltage. A key ingredient of our approach is the photovoltaic effect that quasi-free carriers occupying acceptor LUMO and donor HOMO states are able to produce. Organic dopant molecules such as F4TCNQ and several others (both *n* and *p* type) are available to dope organic semiconductors and may be useful both to facilitate the presence of majority carriers and shield coulomb interactions. Bound states cannot participate in the Fermi level displacement. Finally, we show how recombination mechanisms of quasi-free carriers plays a determining role in establishing the achievable PCE. Electron–hole recombination is analyzed by means of the chemical capacitance, which monitors the electron DOS occupancy, and recombination resistance parameters extracted from IS measurements.

■ ASSOCIATED CONTENT

S Supporting Information. Representative data of capacitance spectroscopy of P3HT:PCBM BHJ solar cells, the role of electrical fields, and transport properties. This material is available free of charge via the Internet at <http://pubs.acs.org>.

■ AUTHOR INFORMATION

Corresponding Author

*E-mail: bisquert@fca.uji.es.

■ BIOGRAPHIES

Juan Bisquert is a professor of applied physics at Universitat Jaume I de Castelló (<http://www.elj.uji.es/jb.php>). He conducts experimental and theoretical research on nanoscale devices for production and storage of clean energies. His main topics of interest are dye- and quantum dot-sensitized solar cells, organic solar cells, and solar fuel production.

Germà Garcia-Belmonte is professor of applied physics at the Universitat Jaume I (Castelló, Spain). Device physics using impedance spectroscopy (modeling and measuring) is his main subject (<http://www.elj.uji.es/ggb.htm>). He conducts research in Organic Electronics as electronic mechanisms in organic light-emitting diodes, organic photovoltaics, and thin-film solar cells.

ACKNOWLEDGMENT

We acknowledge financial support from Ministerio de Ciencia e Innovación under Project HOPE CSD2007-00007, and Generalitat Valenciana under Projects PROMETEO/2009/058, ACOMP/2009/056, and ACOMP/2009/095.

REFERENCES

- (1) Tang, C. W. Two-Layer Organic Photovoltaic Cell. *Appl. Phys. Lett.* **1986**, *48*, 183–185.
- (2) Dennler, G.; Scharber, M. C.; Brabec, C. J. Polymer-Fullerene Bulk-Heterojunction Solar Cells. *Adv. Mater.* **2009**, *21*, 1323–1338.
- (3) Kippelen, B.; Bredas, J.-L. Organic Photovoltaics. *Energy Environ. Sci.* **2009**, *2*, 251–261.
- (4) Liang, Y.; Yu, L. A New Class of Semiconducting Polymers for Bulk Heterojunction Solar Cells with Exceptionally High Performance. *Acc. Chem. Res.* **2010**, *43*, 1227–1236.
- (5) Chen, H.-Y.; Hou, J.; Zhang, S.; Liang, Y.; Yang, G.; Yang, Y.; Yu, L.; Wu, Y.; Li, G. Polymer Solar Cells with Enhanced Open-Circuit Voltage and Efficiency. *Nat. Photonics* **2009**, *3*, 649–653.
- (6) Wienk, M. M.; Kroon, J. M.; Verhees, W. J. H.; Knol, J.; Hummelen, J. C.; van Hal, P. A.; Janssen, R. A. J. Efficient Methano-[70]fullerene/MDMO-PPV Bulk Heterojunction Photovoltaic Cells. *Angew. Chem., Int. Ed.* **2003**, *42*, 3371–3375.
- (7) Padinger, F.; Rittberger, R. S.; Sariciftci, N. S. Effects of Postproduction Treatment on Plastic Solar Cells. *Adv. Funct. Mater.* **2003**, *13*, 85–88.
- (8) Guo, J.; Liang, Y.; Szarko, J.; Lee, B.; Son, H. J.; Rolczynski, B. S.; Yu, L.; Chen, L. X. Structure, Dynamics, and Power Conversion Efficiency Correlations in a New Low Bandgap Polymer: PCBM Solar Cell. *J. Phys. Chem. B* **2010**, *114*, 742–748.
- (9) Clarke, T. M.; Ballantyne, A.; Shoaee, S.; Soon, Y. W.; Duffy, N. W.; Heeney, M.; McCulloch, I.; Nelson, J.; Durrant, J. R. Analysis of Charge Photogeneration as a Key Determinant of Photocurrent Density in Polymer:Fullerene Solar Cells. *Adv. Mater.* **2010**, *22*, 5287–5291.
- (10) Bisquert, J.; Cahen, D.; Rühle, S.; Hodes, G.; Zaban, A. Physical Chemical Principles of Photovoltaic Conversion with Nanoparticulate, Mesoporous Dye-Sensitized Solar Cells. *J. Phys. Chem. B* **2004**, *108*, 8106–8118.
- (11) Irwin, M. D.; Buchholz, D. B.; Hains, A. W.; Chang, R. P. H.; Marks, T. J. p-Type Semiconducting Nickel Oxide as an Efficiency-Enhancing Anode Interfacial Layer in Polymer Bulk-Heterojunction Solar Cells. *Proc. Natl. Acad. Sci. U.S.A.* **2008**, *105*, 2783–2787.
- (12) White, M. S.; Olson, D. C.; Shaheen, S. E.; Kopidakis, N.; Ginley, D. S. Inverted Bulk-Heterojunction Organic Photovoltaic Device Using a Solution-Derived ZnO Underlayer. *Appl. Phys. Lett.* **2006**, *89*, 143517.
- (13) Chen, L.-M.; Hong, Z.; Li, G.; Yang, Y. Recent Progress in Polymer Solar Cells: Manipulation of Polymer:Fullerene Morphology and the Formation of Efficient Inverted Polymer Solar Cells. *Adv. Mater.* **2009**, *21*, 1–16.
- (14) Zhao, D. W.; Tan, S. T.; Ke, L.; Liu, P.; Kyaw, A. K. K.; Sun, X. W.; Lo, G. Q.; Kwong, D. L. Optimization of an Inverted Organic Solar Cell. *Sol. Energy Mater. Sol. Cells* **2010**, *94*, 985–991.
- (15) Boix, P. P.; Ajuria, J.; Etxebarria, I.; Pacios, R.; Garcia-Belmonte, G.; Bisquert, J. Role of ZnO Electron-Selective Layers in Regular and Inverted Bulk Heterojunction Solar Cells. *J. Phys. Chem. Lett.* **2011**, *2*, 407–411.
- (16) Waldauf, C.; Schilinsky, P.; Hauch, J.; Brabec, C. J. Material And Device Concepts for Organic Photovoltaics: Towards Competitive Efficiencies. *Thin Solid Films* **2004**, *451–452*, 503–507.
- (17) Koster, L. J. A.; Smits, E. C. P.; Mihaileti, V. D.; Blom, P. W. M. Device Model for the Operation of Polymer/Fullerene Bulk Heterojunction Solar Cells. *Phys. Rev. B* **2005**, *72*, 085205.
- (18) Deibel, C.; Dyakonov, V. Polymer–Fullerene Bulk Heterojunction Solar Cells. *Rep. Prog. Phys.* **2010**, *73*, 096401.
- (19) Riess, I. What Does a Voltmeter Measure? *Solid State Ionics* **1997**, *95*, 327–328.
- (20) Marshak, A. H. Modeling Semiconductor Devices with Position-Dependent Material Parameters. *IEEE Trans. Electron Devices* **1989**, *36*, 1764–1772.
- (21) Cahen, D.; Kahn, A. Electron Energetics at Surfaces & Interfaces: Concepts And Experiments. *Adv. Mater.* **2003**, *15*, 271.
- (22) Goodman, A. M.; Rose, A. Double Extraction of Uniformly Generated Electron–Hole Pairs from Insulators with Noninjecting Contacts. *J. Appl. Phys.* **1971**, *52*, 2823–2830.
- (23) Sokel, R.; Hughes, R. C. Numerical Analysis of Transient Photoconductivity in Insulators. *J. Appl. Phys.* **1982**, *53*, 7414–7424.
- (24) Blom, P. W. M.; de Jong, M. J. M.; van Munster, M. G. Electric-Field and Temperature Dependence of the Hole Mobility In Poly(p-phenylene vinylene). *Phys. Rev. B* **1997**, *55*, R656.
- (25) Shen, Y.; Hosseini, A. R.; Wong, M. H.; Malliaras, G. G. How to Make Ohmic Contacts to Organic Semiconductors. *ChemPhysChem* **2004**, *5*, 16–25.
- (26) Würfel, P. *Physics of Solar Cells. From Principles to New Concepts*; Wiley: Weinheim, Germany, 2005.
- (27) Kahn, A.; Koch, N.; Gao, W. Electronic Structure and Electrical Properties of Interfaces between Metals and π -Conjugated Molecular Films. *J. Polym. Sci., Part B: Polym. Phys.* **2003**, *41*, 2529.
- (28) Ishii, H.; Sugiyama, K.; Ito, E.; Seki, K. Energy Level Alignment and Interfacial Electronic Structures at Organic/Metal and Organic/Organic Interfaces. *Adv. Mater.* **1999**, *11*, 605.
- (29) Walzer, K.; Maennig, B.; Pfeiffer, M.; Leo, K. Highly Efficient Organic Devices Based on Electrically Doped Transport Layers. *Chem. Rev.* **2007**, *107*, 1233–1271.
- (30) Barea, E. M.; Zafer, C.; Gultein, B.; Aydin, B.; Koyuncu, S.; Icli, S.; Fabregat-Santiago, F.; Bisquert, J. Quantification of The Effects of Recombination and Injection in the Performance of Dye-Sensitized Solar Cells Based on N-Substituted Carbazole Dyes. *J. Phys. Chem. C* **2010**, *114*, 19840–19848.
- (31) Fabregat-Santiago, F.; Garcia-Belmonte, G.; Mora-Seró, I.; Bisquert, J. Characterization of Nanostructured Hybrid and Organic Solar Cells by Impedance Spectroscopy. *Phys. Chem. Chem. Phys.* **2011**, *13*, 9083–9118.
- (32) Bisquert, J. Interpretation of Electron Diffusion Coefficient in Organic and Inorganic Semiconductors with Broad Distributions of States. *Phys. Chem. Chem. Phys.* **2008**, *10*, 3175–3194.
- (33) Abkowitz, M.; Facci, J. S.; Rehm, J. Direct Evaluation of Contact Injection Efficiency into Small Molecule Based Transport Layers: Influence of Extrinsic Factors. *J. Appl. Phys.* **1998**, *83*, 2670–2676.
- (34) Hains, A. W.; Liang, Z.; Woodhouse, M. A.; Gregg, B. A. Molecular Semiconductors in Organic Photovoltaic Cells. *Chem. Rev.* **2010**, *110*, 6689–6735.
- (35) Mora-Seró, I.; Garcia-Belmonte, G.; Boix, P. P.; Vázquez, M. A.; Bisquert, J. Impedance Characterisation of Highly Efficient Silicon Solar Cell under Different Light Illumination Intensities. *Energy Environ. Sci.* **2009**, *2*, 678–686.
- (36) Turrión, M.; Bisquert, J.; Salvador, P. Flatband Potential of F: SnO₂ in a TiO₂ Dye-Sensitized Solar Cell: An Interference Reflection Study. *J. Phys. Chem. B* **2003**, *107*, 9397–9403.
- (37) Choulis, S. A.; Choong, V.-E.; Mathai, M. M.; So, F. The Effect of Interfacial Layer on the Performance of Organic Light-Emitting Diodes. *App. Phys. Lett.* **2005**, *87*, 113503.
- (38) Garcia-Belmonte, G.; Munar, A.; Barea, E. M.; Bisquert, J.; Ugarte, I.; Pacios, R. Charge Carrier Mobility and Lifetime of Organic Bulk Heterojunctions Analyzed by Impedance Spectroscopy. *Org. Electron.* **2008**, *9*, 847–851.
- (39) Abdou, M. S. A.; Orfino, F. P.; Son, Y.; Holdcroft, S. Interaction of Oxygen with Conjugated Polymers: Charge Transfer Complex Formation with Poly(3-alkylthiophenes). *J. Am. Chem. Soc.* **1997**, *119*, 4518.
- (40) Hoshino, S.; Yoshida, M.; Uemura, S.; Kodzasa, T.; Takada, N.; Kamata, T.; Yase, K. Influence of Moisture on Device Characteristics of Polythiophene-Based Field-Effect Transistors. *J. Appl. Phys.* **2004**, *95*, 5088.
- (41) Liang, Z.; Nardes, A.; Wang, D.; Berry, J. J.; Gregg, B. A. Defect Engineering in π -Conjugated Polymers. *Chem. Mater.* **2009**, *21*, 4914–4919.

- (42) Limpinsel, M.; Wagenpfahl, A.; Mingeback, M.; Deibel, C.; Dyakonov, V. Photocurrent in Bulk Heterojunction Solar Cells. *Phys. Rev. B* **2010**, *81*, 085203.
- (43) Gautam, V.; Bag, M.; Narayan, K. S. Dynamics of Bulk Polymer Heterostructure/Electrolyte Devices. *J. Phys. Chem. Lett.* **2010**, *1*, 3277–3282.
- (44) Morfa, A. J.; Nardes, A. M.; Shaheen, S. E.; Kopidakis, N.; van de Lagemaat, J. Time-of-Flight Studies of Electron-Collection Kinetics in Polymer:Fullerene Bulk-Heterojunction Solar Cells. *Adv. Funct. Mater.* **2011**, *21*, 2580–2586.
- (45) Green, M. A.; Shewchun, J. Minority Carrier Effects upon the Small Signal and Steady State Properties of Schottky Diodes. *Solid-State Electron.* **1973**, *16*, 1141–1150.
- (46) Bisquert, J. Chemical Capacitance Of Nanostructured Semiconductors: Its Origin And Significance For Heterogeneous Solar Cells. *Phys. Chem. Chem. Phys.* **2003**, *5*, 5360–5364.
- (47) Garcia-Belmonte, G.; Boix, P. P.; Bisquert, J.; Lenes, M.; Bolink, H. J.; La Rosa, A.; Filippone, S.; Martín, N. Influence of the Intermediate Density-of-States Occupancy on Open-Circuit Voltage of Bulk Heterojunction Solar Cells with Different Fullerene Acceptors. *J. Phys. Chem. Lett.* **2010**, *1*, 2566–2571.
- (48) Garcia-Belmonte, G.; Boix, P. P.; Bisquert, J.; Sessolo, M.; Bolink, H. J. Simultaneous Determination of Carrier Lifetime and Electron Density-of-States in P3HT:PCBM Organic Solar Cells under Illumination by Impedance Spectroscopy. *Sol. Energy Mater. Sol. Cells* **2010**, *94*, 366–375.
- (49) Bisquert, J.; Fabregat-Santiago, F.; Mora-Seró, I.; Garcia-Belmonte, G.; Barea, E. M.; Palomares, E. A Review of Recent Results on Electrochemical Determination of the Density of Electronic States of Nanostructured Metal–Oxide Semiconductors and Organic Hole Conductors. *Inorg. Chim. Acta* **2008**, *361*, 684–698.
- (50) Maurano, A.; Hamilton, R.; Shuttle, C. G.; Ballantyne, A. M.; Nelson, J.; O'Regan, B.; Zhang, W.; McCulloch, I.; Azimi, H.; Morana, M.; Brabec, C. J.; Durrant, J. R. Recombination Dynamics as a Key Determinant of Open Circuit Voltage in Organic Bulk Heterojunction Solar Cells: A Comparison of Four Different Donor Polymers. *Adv. Mater.* **2010**, *22*, 4987–4992.
- (51) Sánchez-Díaz, A.; Izquierdo, M.; Filippone, S.; Martín, N.; Palomares, E. The Origin of the High Voltage in DPM12/P3HT Organic Solar Cells. *Adv. Funct. Mater.* **2010**, *20*, 2695–2700.
- (52) He, Y.; Chen, H.-Y.; Hou, J.; Li, Y. Indene C60 Bisadduct: A New Acceptor for High-Performance Polymer Solar Cells. *J. Am. Chem. Soc.* **2010**, *132*, 1377–1382.
- (53) Dang, X.-D.; Tamayo, A. B.; Seo, J.; Hoven, C. V.; Walker, B.; Nguyen, T.-Q. Nanostructure and Optoelectronic Characterization of Small Molecule Bulk Heterojunction Solar Cells by Photoconductive Atomic Force Microscopy. *Adv. Funct. Mater.* **2010**, *20*, 3314–3321.
- (54) Garcia-Belmonte, G.; Bisquert, J. Open-Circuit Voltage Limit Caused by Recombination through Tail States in Bulk Heterojunction Polymer–Fullerene Solar Cells. *Appl. Phys. Lett.* **2010**, *96*, 113301.
- (55) Scharber, M. C.; Mühlbacher, D.; Koppe, M.; Denk, P.; Waldauf, C.; Heeger, A. J.; Brabec, C. J. Design Rules for Donors in Bulk-Heterojunction Solar Cells—Towards 10% Energy-Conversion Efficiency. *Adv. Mater.* **2006**, *18*, 789–794.
- (56) Cowan, S. R.; Roy, A.; Heeger, A. J. Recombination in Polymer–Fullerene Bulk Heterojunction Solar Cells. *Phys. Rev. B* **2010**, *82*, 245207.
- (57) Guan, Z.-L.; Kim, J. B.; Wang, H.; Jaye, C.; Fisher, D. A.; Loo, Y. L.; Kahn, A. Direct Determination of the Electronic Structure of the Poly(3-hexylthiophene):Phenyl-[6,6]-C61 Butyric Acid Methyl Ester Blend. *Org. Electron.* **2010**, *11*, 1779–1785.
- (58) Kaake, L. G.; Barbara, P. F.; Zhu, X. Y. Intrinsic Charge Trapping in Organic and Polymeric Semiconductors: A Physical Chemistry Perspective. *J. Phys. Chem. Lett.* **2010**, *1*, 628–635.
- (59) Pomerantz, Z.; Zaban, A.; Ghosh, S.; Lellouche, J.-P.; Garcia-Belmonte, G.; Bisquert, J. Capacitance, Spectroelectrochemistry and Conductivity of Polarons and Bipolarons in a Polydicarbazole Based Conducting Polymer. *J. Electroanal. Chem.* **2008**, *614*, 49–60.
- (60) Pensack, R. D.; Asbury, J. B. Beyond the Adiabatic Limit: Charge Photogeneration in Organic Photovoltaic Materials. *J. Phys. Chem. Lett.* **2010**, *1*, 2255–2263.
- (61) Shockley, W.; Queisser, H. J. Detailed Balance Limit Of Efficiency Of P–N Junction Solar Cells. *J. Appl. Phys.* **1961**, *32*, S10.
- (62) Street, R. A.; Cowan, S.; Heeger, A. J. Experimental Test for Geminate Recombination Applied to Organic Solar Cells. *Phys. Rev. B* **2010**, *82*, 121301(R).
- (63) Shuttle, C. G.; Hamilton, R.; O'Regan, B. C.; Nelson, J.; Durrant, J. R. Charge-Density-Based Analysis of the Current–Voltage Response of Polythiophene/Fullerene Photovoltaic Devices. *Proc. Natl. Acad. Sci. U.S.A.* **2010**, *107*, 16448–16452.
- (64) Sun, S.-S. Optimal Energy Offsets for Organic Solar Cells Containing a Donor/Acceptor Pair. *Sol. Energy Mater. Sol. Cells* **2005**, *85*, 261–267.
- (65) Godovsky, D. Modeling the Ultimate Efficiency of Polymer Solar Cell Using Marcus Theory of Electron Transfer. *Org. Electron.* **2011**, *12*, 190–194.
- (66) Boix, P. P.; Ajuria, J.; Pacios, R.; Garcia-Belmonte, G. Carrier Recombination Losses in Inverted Polymer:Fullerene Solar Cells With ZnO Hole-Blocking Layer From Transient Photovoltage and Impedance Spectroscopy Techniques. *J. Appl. Phys.* **2011**, *109*, 074514.
- (67) Bisquert, J.; Fabregat-Santiago, F.; Mora-Seró, I.; Garcia-Belmonte, G.; Giménez, S. Electron Lifetime in Dye-Sensitized Solar Cells: Theory and Interpretation of Measurements. *J. Phys. Chem. C* **2009**, *113*, 17278–17290.
- (68) Lin Leong, W.; Cowan, S. R.; Heeger, A. J. Differential Resistance Analysis of Charge Carrier Losses in Organic Bulk Heterojunction Solar Cells: Observing the Transition from Bimolecular to Trap-Assisted Recombination and Quantifying the Order of Recombination. *Adv. Ener. Mat.* **2011** 10.1002/aenm.201100196.
- (69) Bisquert, J.; Mora-Seró, I. Simulation of Steady-State Characteristics of Dye-Sensitized Solar Cells and the Interpretation of the Diffusion Length. *J. Phys. Chem. Lett.* **2010**, *1*, 450–456.
- (70) Donolato, C. A Reciprocity Theorem for Charge Collection. *Appl. Phys. Lett.* **1985**, *46*, 270–272.
- (71) Rau, U. Reciprocity Relation between Photovoltaic Quantum Efficiency and Electroluminescent Emission of Solar Cells. *Phys. Rev. B* **2007**, *76*, 085303.
- (72) Maurano, A.; Shuttle, C. G.; Hamilton, R.; Ballantyne, A.; Nelson, J.; Zhang, W.; Heeney, M.; Durrant, J. R. Charge Photogeneration in Low Band Gap Polyselenophene/Fullerene Blend Films. *J. Phys. Chem. C* **2011**, *114*, 8068–8075.
- (73) Jonathan, D. S.; Mark, A. R.; Tobin, J. M. Practical Efficiency Limits in Organic Photovoltaic Cells: Functional Dependence of Fill Factor and External Quantum Efficiency. *Appl. Phys. Lett.* **2009**, *95*, 163302.
- (74) Marsh, R. A.; Hodgkiss, J. M.; Friend, R. H. Direct Measurement of Electric Field-Assisted Charge Separation in Polymer:Fullerene Photovoltaic Diodes. *Adv. Mater.* **2010**, *22*, 3672–3676.
- (75) Clarke, T. M.; Ballantyne, A. M.; Tierney, S.; Heeney, M.; Duffy, W.; McCulloch, I.; Nelson, J.; Durrant, J. R. Charge Photogeneration in Low Band Gap Polyselenophene/Fullerene Blend Films. *J. Phys. Chem. C* **2010**, *114*, 8068–8075.
- (76) Shuttle, C. G.; O'Regan, B.; Ballantyne, A. M.; Nelson, J.; Bradley, D. D. C.; Durrant, J. R. Bimolecular Recombination Losses in Polythiophene:Fullerene Solar Cells. *Phys. Rev. B* **2008**, *78*, 113201.
- (77) Banerji, N.; Cowan, S.; Leclerc, M.; Vauthey, E.; Heeger, A. J. Exciton Formation, Relaxation, and Decay in PCDTBT. *J. Am. Chem. Soc.* **2010**, *132*, 17459–17470.
- (78) Brédas, J.-L.; Norton, J. E.; Cornil, J.; Coropceanu, V. Molecular Understanding of Organic Solar Cells: The Challenges. *Acc. Chem. Res.* **2009**, *42*, 1691–1699.
- (79) Clarke, T. M.; Durrant, J. R. Charge Photogeneration in Organic Solar Cells. *Chem. Rev.* **2010**, *110*, 6736–6767.
- (80) Morteani, A. C.; Sreearunothai, P.; Herz, L. M.; Friend, R. H.; Silva, C. Exciton Regeneration at Polymeric Semiconductor Heterojunctions. *Phys. Rev. Lett.* **2004**, *92*, 247402.

(81) Vandewal, K.; Tvingstedt, K.; Gadisa, A.; Inganäs, O.; Manca, J. V. On the Origin of the Open-Circuit Voltage of Polymer–Fullerene Solar Cells. *Nat. Mater.* **2009**, *8*, 904–909.

(82) Clarke, T. M.; Ballantyne, A.; Shoaee, S.; Soon, Y. W.; Duffy, W.; Heeney, M.; McCulloch, I.; Nelson, J.; Durrant, J. R. Analysis of Charge Photogeneration as a Key Determinant of Photocurrent Density in Polymer: Fullerene Solar Cells. *Adv. Mater.* **2010**, *22*, 5287–5291.

(83) Mahan, G. D. Excitons in Degenerate Semiconductors. *Phys. Rev.* **1967**, *153*, 882.

(84) Gay, J. G. Screening of Excitons in Semiconductors. *Phys. Rev. B* **1971**, *4*, 2567.

(85) Shields, A. J.; Pepper, M.; Ritchie, D. A.; Simmons, M. Y.; Jones, G. A. C. Quenching of Excitonic Optical Transitions by Excess Electrons in GaAs Quantum Wells. *Phys. Rev. B* **1995**, *51*, 18049.

(86) Banyai, L.; Koch, S. W. Absorption Blue Shift in Laser-Excited Semiconductor Microspheres. *Phys. Rev. Lett.* **1986**, *57*, 2722.

(87) Deibel, C.; Strobel, T.; Dyakonov, V. Origin of the Efficient Polaron-Pair Dissociation in Polymer–Fullerene Blends. *Phys. Rev. Lett.* **2009**, *103*, 036402.

(88) Arkhipov, V. I.; Heremans, P.; Bäessler, H. Why is Exciton Dissociation So Efficient at the Interface Between a Conjugated Polymer and an Electron Acceptor? *Appl. Phys. Lett.* **2003**, *82*, 4605–4607.

(89) Wiemer, M.; Nenashev, A. V.; Jansson, F.; Baranovskii, S. D. On the Efficiency of Exciton Dissociation at the Interface between a Conjugated Polymer and an Electron Acceptor. *Appl. Phys. Lett.* **2011**, *99*, 013302.

(90) Biju, V.; Barazzouk, S.; Thomas, K. G.; George, M. V.; Kamat, P. V. Photoinduced Electron Transfer between 1,2,5-Triphenylpyrrolidinofullerene Cluster Aggregates and Electron Donors. *Langmuir* **2001**, *17*, 2930–2936.

(91) Biju, V.; Sudeep, P. K.; Thomas, K. G.; George, M. V.; Barazzouk, S.; Kamat, P. V. Clusters of Bis- and Tris-Fullerenes. *Langmuir* **2002**, *18*, 1831–1839.

(92) Agostinelli, T.; Lilliu, S.; Labram, J. G.; Campoy-Quiles, M.; Hampton, M.; Pires, E.; Rawle, J.; Bikondoa, O.; Bradley, D. D. C.; Anthopoulos, T. D.; Nelson, J.; Macdonald, J. E. Real-Time Investigation of Crystallization and Phase-Segregation Dynamics in P3HT: PCBM Solar Cells During Thermal Annealing. *Adv. Funct. Mater.* **2011**, *21*, 1701–1708.